Neurobiology of Disease 141 (2020) 104880

Contents lists available at ScienceDirect

Neurobiology of Disease

journal homepage: www.elsevier.com/locate/ynbdi

A homozygous *MRPL24* mutation causes a complex movement disorder and affects the mitoribosome assembly

Michela Di Nottia[a,1], Maria Marchese[b,1], Daniela Verrigni[a], Christian Daniel Mutti[c], Alessandra Torraco[a], Romina Oliva[d], Erika Fernandez-Vizarra[c], Federica Morani[b], Giulia Trani[a], Teresa Rizza[a], Daniele Ghezzi[e,f], Anna Ardissone[g,h], Claudia Nesti[b], Gessica Vasco[i], Massimo Zeviani[c], Michal Minczuk[c], Enrico Bertini[a], Filippo Maria Santorelli[b,2], Rosalba Carrozzo[a,*,2]

[a] Unit of Muscular and Neurodegenerative Disorders, Laboratory of Molecular Medicine, Bambino Gesù Children's Hospital, IRCCS, Rome, Italy
[b] Molecular Medicine & Neurogenetics, IRCCS Fondazione Stella Maris, Pisa, Italy
[c] MRC Mitochondrial Biology Unit, University of Cambridge, Cambridge, UK
[d] Department of Sciences and Technologies, University Parthenope of Naples, Naples, Italy
[e] Unit of Medical Genetics and Neurogenetics, Fondazione IRCCS Istituto Neurologico Carlo Besta, Milan, Italy
[f] Department of Pathophysiology and Transplantation, University of Milan, Milan, Italy
[g] Child Neurology Unit, Fondazione IRCCS Istituto Neurologico Carlo Besta, Milan, Italy
[h] Department of Molecular and Translational Medicine DIMET, University of Milan-Bicocca, Milan, Italy
[i] Department of Neurosciences, IRCCS Bambino Gesù Children Hospital, Rome, Italy

ARTICLE INFO

Keywords:
Mitochondrial disorders
Movement disorder
MRPL24
Mitoribosomes
Mitochondrial protein synthesis
Zebrafish
Molecular modeling
Protein interactions

ABSTRACT

Mitochondrial ribosomal protein large 24 (MRPL24) is 1 of the 82 protein components of mitochondrial ribosomes, playing an essential role in the mitochondrial translation process.

We report here on a baby girl with cerebellar atrophy, choreoathetosis of limbs and face, intellectual disability and a combined defect of complexes I and IV in muscle biopsy, caused by a homozygous missense mutation identified in *MRPL24*. The variant predicts a Leu91Pro substitution at an evolutionarily conserved site. Using human mutant cells and the zebrafish model, we demonstrated the pathological role of the identified variant. In fact, in fibroblasts we observed a significant reduction of MRPL24 protein and of mitochondrial respiratory chain complex I and IV subunits, as well a markedly reduced synthesis of the mtDNA-encoded peptides. In zebrafish we demonstrated that the orthologue gene is expressed in metabolically active tissues, and that gene knockdown induced locomotion impairment, structural defects and low ATP production. The motor phenotype was complemented by human WT but not mutant cRNA. Moreover, sucrose density gradient fractionation showed perturbed assembly of large subunit mitoribosomal proteins, suggesting that the mutation leads to a conformational change in MRPL24, which is expected to cause an aberrant interaction of the protein with other components of the 39S mitoribosomal subunit.

1. Introduction

Mammalian Mitochondrial Ribosomal Proteins (MRPs) are encoded by nuclear genes and are required for the translation of the 13 mtDNA-encoded proteins within the mitochondrion. Mitochondrial ribosomes (mitoribosomes) consist of a small 28S subunit and a large 39S subunit. The human MRP gene family comprises 30 genes encoding for the small mitochondrial ribosomal subunit and 52 genes for the large subunit, all of which are nuclear encoded (Gopisetty and Thangarajan, 2016). Building a mitoribosome is a difficult logistical task comparable to the complexity of assembling the entire respiratory chain, since the biogenesis of mitoribosomes depends on the coordinated synthesis of

* Corresponding author at: Unit of Muscular and Neurodegenerative Disorders, Laboratory of Molecular Medicine, Bambino Gesù Children's Hospital, IRCCS, Viale di San Paolo 15, 00146 Rome, Italy.
E-mail address: rosalba.carrozzo@opbg.net (R. Carrozzo).
[1] These authors contributed equally to this work.
[2] These authors contributed equally as senior authors.

https://doi.org/10.1016/j.nbd.2020.104880
Received 12 July 2019; Received in revised form 4 March 2020
Available online 25 April 2020

MRPs, which must be translated on cytoplasmic ribosomes and imported into mitochondria (Bogenhagen et al., 2018). Mitoribosomes are essential for the synthesis of the oxidative phosphorylation machinery. It has indeed been proposed that the absence or deficiency of MRPs may cause primary oxidative phosphorylation disorders (O'Brien et al., 2000). The consequences of mutations in MRP genes are expected to reproduce the clinical heterogeneity of oxidative phosphorylation disorders, ranging from lethality to less severe phenotypes associated with marginally impaired energy metabolism, as mutations that do not fully inactivate the protein function may have intermediate effects (O'Brien et al., 2005). In addition, mutations in MRP genes could cause tissue-specific disorders (Spirina et al., 2000). The crucial role of mitoribosomes in OXPHOS biogenesis underlines the involvement of MRPs in a number of conditions associated with mitochondrial dysfunction (Bieri et al., 2018). The importance of the proper composition and structure of mitoribosomes for human health has led to their recent structural characterization, which provided detailed insight in the protein-rich mammalian mitoribosome (Amunts et al., 2015; Greber et al., 2015), and a structure-based kinetic model for its assembly (Bogenhagen et al., 2018). Finally, very recently, dysfunction of these proteins has been demonstrated to play a role not only in the primary mitochondrial respiratory chain activity deficiencies, but also in other conditions, such as cancer, impaired development, neurodegeneration, cardiovascular failure, obesity and inflammatory disorders (Gopisetty and Thangarajan, 2016).

Mitochondrial ribosomal protein large 24 (MRPL24) is one of the protein components of the large (39S) subunit of mitochondrial ribosomes (Kenmochi et al., 2001). Herein, we report on the first case with mutation in *MRPL24* and provide a comprehensive investigation of its clinical, biochemical and structural consequences. We demonstrated the pathological role of the identified variant using human mutant cells. Moreover, we evaluated the consequence of a dysfunctional Mrlp24 in the developing zebrafish embryos, in order to determine the impact on early stages of development.

2. Material and methods

2.1. Standard protocol approvals, registrations, and patient consent

The study was approved by the Ethical Committees of the Bambino Gesù Children Hospital, Rome, Italy, in agreement with the Declaration of Helsinki. Informed consent was signed by the parents of the patient.

2.2. Mutational analysis

Total genomic DNA underwent targeting resequencing (BGI-Shenzhen, Shenzhen, China) using a customized probe library (Agilent SureSelectXT Custom Kit) designed to capture the coding exons and 20 nucleotides of flanking introns of 1381 genes coding for mitochondrial proteins ("Mitoexome") (Calvo et al., 2012). Deep sequencing used an Illumina Hiseq technology, with a 255× effective mean depth. The Burrows-Wheeler Aligner (BWA, http://bio-bwa.sourceforge.net/) software was applied for analysis, classification, and reporting of genomic variants. After excluding previously annotated single nucleotide changes occurring with high frequency in populations (> 1%), we prioritized variants predicted to have a functional impact (i.e., non-synonymous variants and changes affecting splice sites). Validation of the *MRPL24* variant and segregation along the family was performed by Sanger Sequencing, using BigDye chemistry 3.1 and run on an ABI 3130XL automatic sequencer (Applied Biosystems, Life Technologies).

2.3. Human samples, biochemical and protein studies

Quadriceps muscle biopsy was obtained for diagnostic spectrophotometric procedures (Bugiani et al., 2004). Human fibroblasts, obtained from skin biopsy, were grown in high glucose DMEM with glutamine supplemented with sodium pyruvate (0.11 g/L) 10% fetal bovine serum, and 50 μg/mL uridine. Complex V activity (in the direction of ATP synthesis) was measured in fibroblast mitochondria, using reported spectrophotometric methods (Rizza et al., 2009). Oxygen consumption rate (OCR) was measured in adherent fibroblasts with an XFe24 Extracellular Flux Analyzer (Seahorse Bioscience,Agilent, Santa Clara, CA), as described in Tolomeo et al., 2019. Western blotting using monoclonal antibodies complex I – NDUFA9 and NDUFS1; complex II – SDHA; complex III – UQCRC2; complex IV – COXIV; complex V – ATP5A1, and porin (VDAC) was performed using precast 4–12% denaturating gels (Bolt™ 4–12% Bis-Tris Plus Gels, Thermo Fisher Scientific, Waltham, MA USA) as reported (Torraco et al., 2018). All monoclonal antibodies were from MitoSciences (Eugene, OR, USA). The polyclonal ab-MRPL24 was from Abcam (Cambridge, UK).

Analysis of mitochondrial protein synthesis was performed as previously described (Chomyn, 1996; Fernández-Silva et al., 2007). Immortalized fibroblasts at 70% confluence were labeled for 1 h with [^{35}S]-L-methionine in the presence of 100 μg/mL emetine, an inhibitor of cytosolic protein synthesis. Samples were kept at −80 °C until use. Twenty μg of total cellular protein were loaded on a Novex™ 18% Tris-Glycine precast SDS polyacrylamide gel (Invitrogen). The gel was then fixed and dried, and the mitochondrial translation products were visualized using a Storage Phosphor Screen and a Typhoon 9410 Variable Mode Imager (GE Healthcare).

For all experiments, age-matched controls were used.

2.4. Model building and in silico analysis

For the analysis of the MRPL24 structure in the context of human mitoribosome, the structure of the entire mitoribosome solved by electron microscopy at a resolution of 3.5 Å was used (PDB ID: 3j9m, Amunts et al., 2015). As the coordinates of the MRPL24 159–168 fragment are missing from this structure, they were comparatively modeled with Modeller9v17 (Sali and Blundell, 1993), using as template the structure of the 89% sequence identical homologous protein from *Sus scrofa* (PDB ID: 4v19, Greber et al., 2014a, 2014b). To simulate the structural effect of the Leu91Pro mutation, Leu91 was mutated to Pro and its phi (ϕ) dihedral angle was set at −63° with PyMol (DeLano, 2002): 63° is indeed the ϕ value typically assumed by prolines in proteins (with variations within ± 15°, MacArthur and Thornton, 1991). The analysis of the interface areas and of the inter-residue contacts between MRPL24 and other proteins/RNAs on the mitoribosome was carried out with CoCoMaps (Vangone et al., 2011).

2.5. Analysis of the mitochondrial ribosome profile on sucrose density gradients

Sedimentation and analysis of the mitochondrial ribosome was performed essentially as described in (Rorbach et al., 2016). Briefly, control or Patient MRPL24 immortalized fibroblast cells were lysed and loaded equally on separate linear sucrose gradients (10–30%) in 50 mM Tris–HCl (pH 7.2), 20 mM $Mg(OAc)_2$, 100 mM NaCl, and centrifuged for 2 h 15 min at 39,000 rpm. Fractions of 100 μL each were collected, and 30 μL of each fraction was analyzed by western blotting using mtLSU antibodies. The fractions within the blots were quantified using ImageJ and normalized to the overall Control/Patient intensity ratio.

2.6. Functional studies in zebrafish

Adult male and female wild-type (WT) zebrafish (AB strains) and transgenic line expressing GFP under a strong cardiac promoter, *Tg (cmlc2:gfp)* (Huang et al., 2003) were maintained according to standard procedures (Westerfield, 2000) on a 14 h light:10 h dark cycle. Zebrafish embryos and larvae procedures complied with the guidelines of our institutional animal care committee, and experiments were

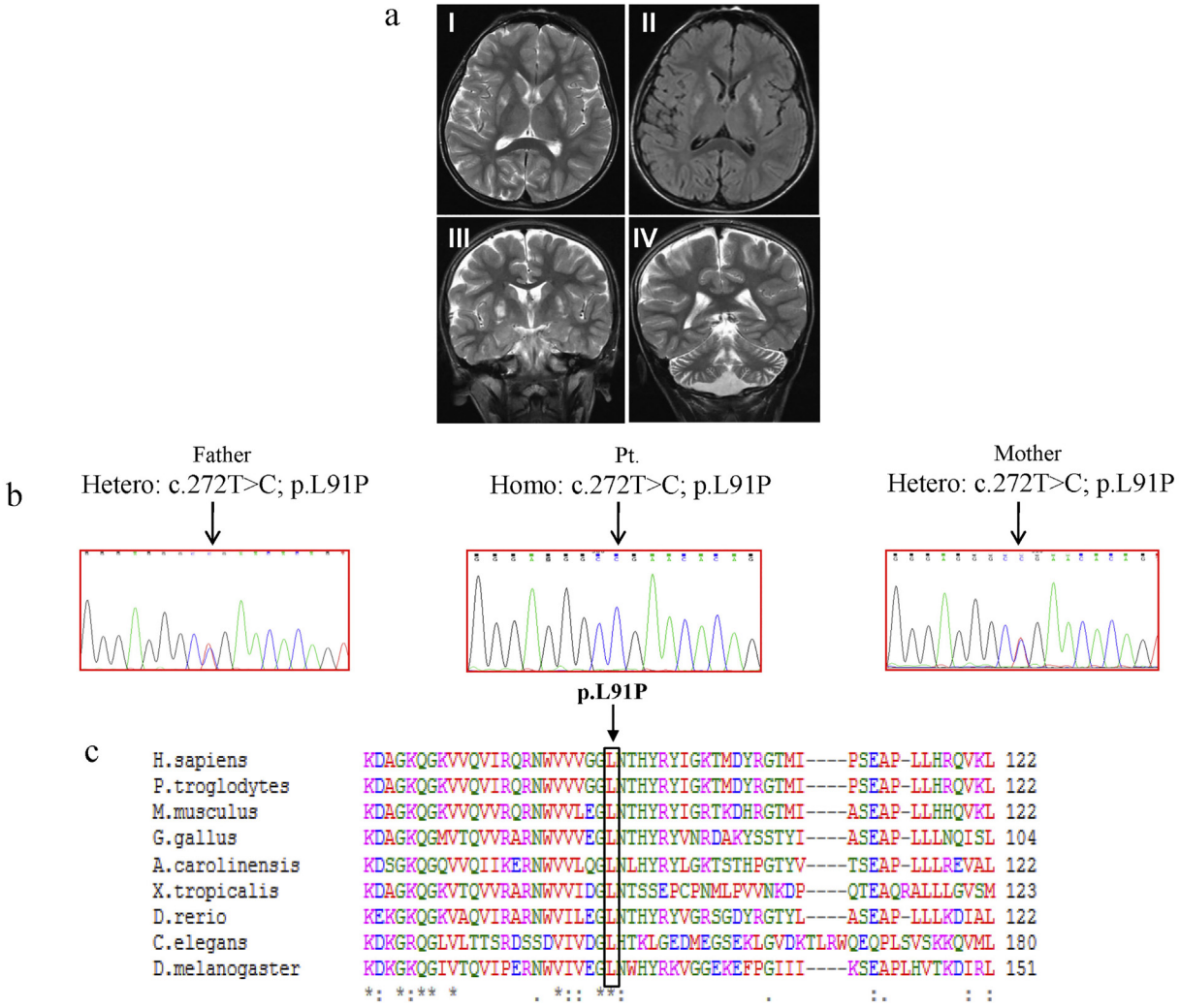

Fig. 1. Brain MRI and genetic features of the MRPL24 patient. a. Brain MRI performed at age 3 years: (I) Axial T2 weighted image; (II) Axial FLAIR weighted image; (III, IV) Coronal T2 weighted images. High intense T2 and FLAIR abnormalities corresponding to the putamen bilaterally are evident in a, b and c. Cerebellar atrophy is shown in d. b. Electropherograms of the genomic region of the patient (Pt) and the parents showing the c.272T > C variant in exon 2 of *MRPL24*. c. Protein sequence alignment (ClustalW) highlights the mutation (p.Leu91Pro; red) in the human MRPL24. The Leu91 is conserved in the invertebrate and vertebrate orthologs. (For interpretation of the references to colour in this figure legend, the reader is referred to the web version of this article.)

performed in accordance with, and under the supervision of, the Institutional Animal Care and Use Committee (IACUC) of the University of Pisa and the Italian National Research Council Institute of Clinical Physiology (CNR-IFC). Every effort was made to minimize both animal suffering and the number of animals needed to collect reliable scientific data.

Total RNA was extracted using the Quick RNA miniprep (Zymo Research, Irvine, USA) from embryos at 48 h post fertilization (hpf) and reversely transcribed using the Transcriptor First Strand cDNA Synthesis Kit (Roche, Hamburg, Germany). Primers for mRNA sequences were designed using the zebrafish sequence of *mrpl24* (ENSDART00000010862.6), and the human transcript (ENST00000361531.6 1). PCR products were cloned into pCS2+ vector and verified for accuracy using capillary sequencing.

Whole mount in situ hybridization (WISH) was performed as described (Thisse and Thisse, 2008) at the 48, 72, and 96-hpf time points. Antisense riboprobe synthesis was performed using the Digoxigenin (DIG) RNA Labeling Kit (Roche). Quantitative reverse transcription followed by the polymerase chain reaction in real time (qRT-PCR) expression analyses was done as described (Marchese et al., 2016).

For the generation of zebrafish *mrpl24* knockdown, we designed morpholino antisense oligonucleotides (MOs) (GeneTools, Philomath, OR) targeting either translation start site (tblockMO) or transcription at exon 4–5 splice site (spliceMO). The MO and primers sequences are listed in Supplementary Table 1. Concentrations of MOs were carefully titrated to avoid nonspecific binding effects and a scrambled control MO was used at similar concentrations to assess specificity to *mrpl24*. After titration, we used in all experiments 3 ng of spliceMO against *mrpl24*. The effect of the MO was evaluated through RT-PCR. Survival was calculated comparing death rates between microinjected and non-injected embryos. Rescue experiments were performed through co-injection of 50 pg of control, *mrpl24* and either human WT or mutant ($mut^{Leu91Pro}$) cRNAs with spliceMO at the same concentration used for the knockdown experiments. Each experiment was repeated at least three times if not otherwise stated.

Birefringence assay in 48 hpf embryos was used to test muscle structure and compaction (Smith et al., 2013). Heart development was analyzed using the *Tg(clmc2:GFP)* embryos anesthetized with 0.04 mg of tricaine (E1052, Sigma) and set down on glass slides embedded in 1.2% low melting agarose (Agarose low gelling, Sigma). The fluorescence imaging was carried out using the Nikon Eclips E600 microscope, and acquired with CoolSnap-CF camera using NIS elements software version 2. For whole mount staining, dechorionated embryos were fixed in 4% PFA overnight and Oil-Red-O (ORO) staining was performed as

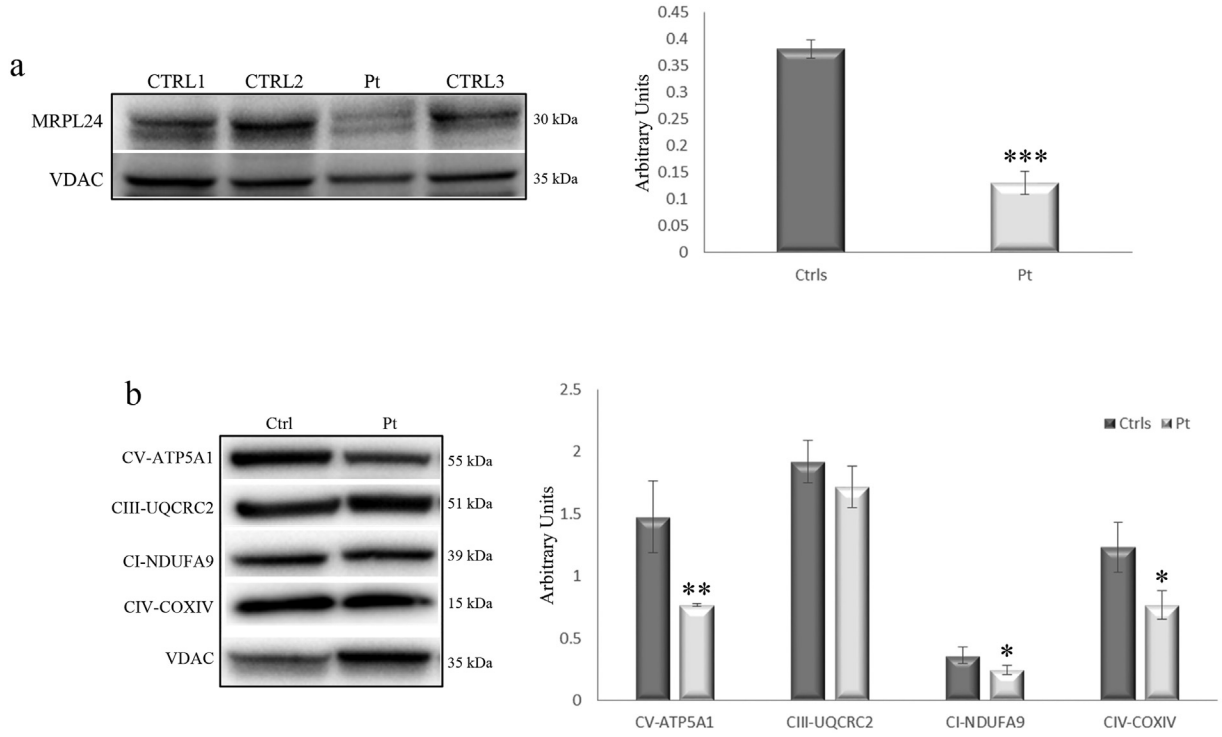

Fig. 2. Decreased levels of MRPL24 and OXPHOS subunits in MRPL24 patient muscle. a, b. Muscle homogenate from controls (Ctrls, $n = 3$) and MRPL24 patient (Pt) was separated on a 4–12% SDS-PAGE and proteins were visualized by western blot analysis using specific antibodies against MRPL24. The same samples were tested for the expression of subunits of the CI (NDUFA9), CIII (UQCRC2), CIV (COXIV), CV (F1β). The levels of the different proteins were normalized to VDAC (corresponding histograms). Data are presented as a mean ± SD of at least three independent experiments; $*p < .05$; $**p < .001$; $***p < .0001$.

described (Fraher et al., 2016). Images were acquired on a Leica M80 microscope with a Nikon Digital Sight DS-Fi1 camera and the NIS Elements software package (Nikon, Nikon Corp., Europe).

Touch-evoked escape response was measured at 48 hpf on a semi-quantitative arbitrary scale from 0 to 2, where 0 is no movement, 1 is flicker of movement but no swimming, and 2 is normal swimming (Marchese et al., 2016).

Western blotting in zebrafish used a polyclonal anti-MRPL24 (1:500), an anti-Total Oxphos (1:1000, Mitoprofile), an anti-complex I (1:1000, Mitosciences), and anti-β-tubulin (1:1000, Cell Signaling) as control.

Oxygen consumption rates in 48-hpf control embryos and morphants ($n = 10$ per group) were measured using an extracellular flux analyzer (XFe24, Seahorse Biosciences) as described (Gibert et al., 2013). Single embryos were placed in individual wells of a 24-well islet plate and a fine screen mesh was used to maintain the larvae in place.

All the sequences of the primers and morpholino used are available in the Supplementary table 1.

2.7. Statistical analysis

All data were analyzed applying either parametric or non-parametric analyses. Homogeneity of variance was assessed using the Levene test. Post hoc comparisons were performed by Mann-Whitney test with Bonferroni's correction, or Unpaired *t*-test following non-parametric analysis of variance. ANOVA with Tukey's Multiple Comparison Test and Fisher's exact and Chi-square test were used in specific zebrafish experiments.

For functional studies on human samples, data are presented as mean ± SD. The Student's t-test was used for the analysis of statistical significance.

3. Results

3.1. Clinical features and brain NMR findings

The patient was the single daughter of healthy unrelated parents. Motor milestones were reported normal until the age of 8 months when she almost acquired sitting position, but within a few weeks, she lost the ability of sitting with support, and vocalisation. She was admitted to our Hospital for the first time at 3 years of age, and clinically she was not able to sit with support and was lying in supine position, showing spasticity and dystonic posturing of distal upper and lower limbs together with dyskinetic facial grimacing. At that time, the MRI showed T2 and FLAIR hyperintense bilateral alterations at the level of the putamen and cerebellar atrophy (Fig. 1A). The child was evaluated again at the age of 8 years and was able to sit with support; but she had intellectual disability with lack of interaction with the environment and aspects of a pervasive behavior. Neurological examination at this age showed choreoathetosis of limbs and face. Increased lactate was detected in blood 2.2 mM (n.v.: 0.9–1.8 mM). Respiratory chain complexes (RCCs) analysis in muscle biopsy revealed multiple defects [RCCIV (−62%), RCCI (−40%) and RCCIII (−42%)]. A second biopsy was performed 3 years later and confirmed the RCCIV defect (−58%), while the other RCC activities were in the control range. Molecular genetic analysis in the muscle tissue excluded deletions and depletion of the mitochondrial DNA. The girl was re-assessed at the age of 14 years and, although she was relatively stable, she could not stand and was wheelchair bound; choreoathetosis persisted with spastic-dystonic tetraparesis. Although the patient was not able to speak, her interaction with the environment had improved, particularly after she had been put in treatment with Idebenone at the dose of 180 mg/day. The electrocardiogram disclosed a RS of 91 bpm, ventricular pre-excitation with associated repolarization anomalies, QTc within limits; the child never had symptoms of a paroxysmal tachycardia in the clinical history. Echocardiogram was normal, though a Holter ECG confirmed findings

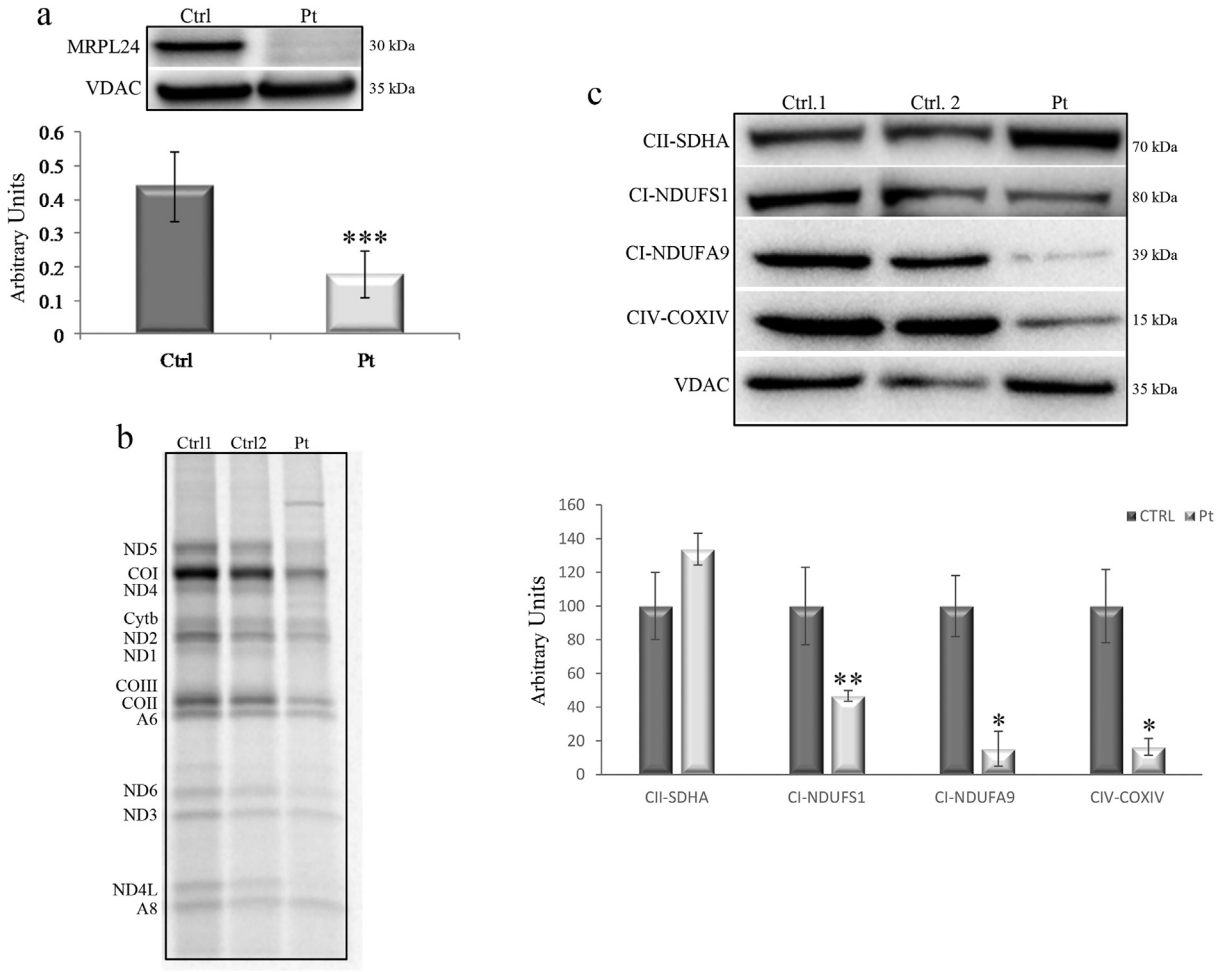

Fig. 3. Decreased levels of MRPL24 and OXPHOS subunits, as well mitochondrial protein synthesis in MRPL24 patient fibroblasts. a, c. Fibroblasts homogenate from controls (Ctrls, $n = 2$) and MRPL24 patient (Pt) was separated on a 4–12% SDS-PAGE and proteins were visualized by western blot analysis using specific antibodies against MRPL24. The same samples were tested for the expression of subunits of the CI (NDUFA9; NDUFS1), CII (SDHA), CIV (COXIV). The levels of the different proteins were normalized to VDAC (corresponding histograms). Data are presented as a mean ± SD of at least three independent experiments; $*p < .05$; $**p < .001$; $***p < .0001$. b. Mitochondrial translation study in two controls and the mutant immortalized fibroblasts cell lines. The experiment was repeated twice in two different batches of cells showing the same result.

suggestive of a Wolff-Parkinson-White syndrome without any other arrhythmia. She is currently on therapy with Riboflavin 200 mg/day, Carnitine 1 g/day, and Idebenone 180 mg/day with the recommendation of careful cardiac monitoring.

3.2. MitoExome and Sanger sequencing

Bioinformatic analysis carried out on a MitoExome targeted panel, on the hypothesis of a recessive trait, identified biallelic mutations in a single gene, *MRPL24* (NC_000001.11). Sanger sequencing confirmed the presence of the c.272T > C (p.Leu91Pro) variant in a homozygous state in the patient and in heterozygosity in her healthy parents (Fig. 1b). The mutation was located in exon 2 and was not reported in public databases (dbSNP (http://www.ncbi.nlm.nih. gov/sites/), ExAC (http://exac.broadinstitute.org/), EVS (http://evs.gs.washington.edu/EVS/), and gnomADv2.1 (http://gnomad.broadinstitute.org), and in *in-house* databases. In silico analysis with Polyphen-2 (PPH2, http://genetics.bwh.harvard.edu/pph2/), SIFT (http://sift.jcvi.org), and Mutation Taster (http://www.mutationtaster.org) predicted a harmful effect of the p.Leu91Pro variant which affects a residue conserved along all the invertebrate and vertebrate phyla (Fig. 1c).

3.3. Functional studies on human samples

The level of MRPL24 protein was dramatically reduced in muscle homogenate (Fig. 2a) associated with a decreased level of subunits of complexes I, IV and V, when normalized with the mitochondrial marker VDAC (Fig. 2b). The fibroblasts showed a significant reduction of the amount of MRPL24 protein as well (Fig. 3a). Specific ^{35}S labelling of the mtDNA-encoded peptides revealed markedly reduced synthesis of all of them in the mutant immortalized fibroblasts (Fig. 3b), and overlapping results were obtained measuring the amount of MRC subunits by western blot (Fig. 3c). In addition, biochemical analysis on fibroblast mitochondria documented a defect of complex V activity using either succinate, malate or pyruvate + malate as substrate (Fig. S1). Using microscale oxygraphy to evaluate the impact of the mutation on mitochondrial respiration we observed significantly reduced basal and maximal respiratory capacities, together with a low mitochondrial ATP output (Fig. S2).

3.4. In silico characterization of MRPL24 mutation

Human MRPL24 is a 216 amino acid protein, highly interconnected with other components of the human mitoribosomal large subunit. It spans a length of over 15 nm on the surface of the large 39S

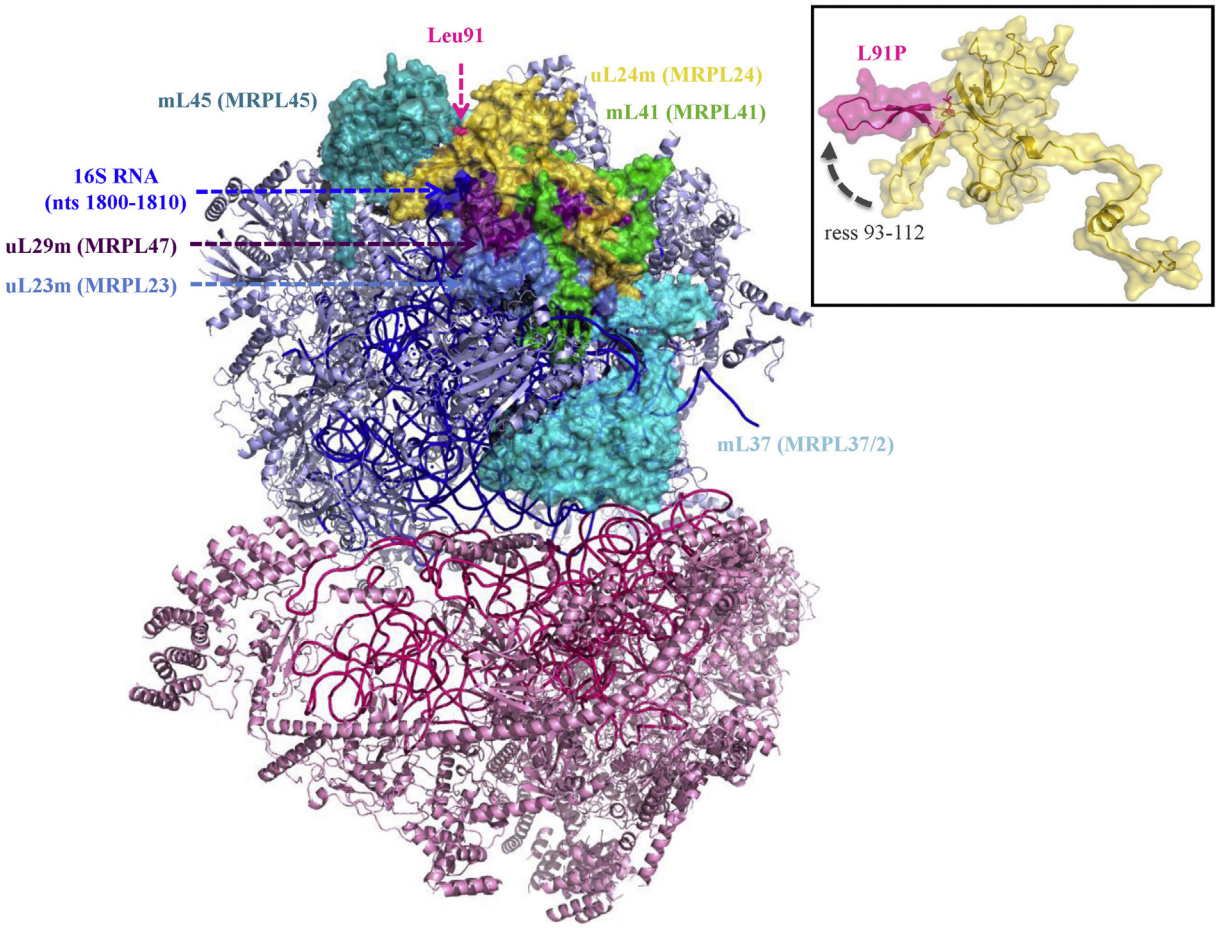

Fig. 4. Three-dimensional representation of the entire human mitoribosome (PDB ID: 3j9m). MRPL24 and all the protein/RNA components it interacts with are shown in a surface representation and labeled. For 16S RNA, only the surface of nucleotides 1800–1810 is shown, for the sake of clarity. The rest of the ribosome is shown in a cartoon representation, with proteins colored pink if in the small and lightblue if in the large subunit and RNAs colored hotpink in the small and deepblue in the large subunit. Inset: MRPL24 is shown in the same orientation as in the mitoribosome. The hypothetical orientation of the beta hairpin motif involving residues Thr93-Glu112, in the Leu91Pro mutant is also shown, colored in hotpink. It was obtained by setting the value of the ϕ dihedral angle of residue 91 to −63° that is the typical accepted value for prolines. (For interpretation of the references to colour in this figure legend, the reader is referred to the web version of this article.)

mitoribosome subunit, where it interacts with five proteins, uL29m (MRPL47), mL41 (MRPL41), uL23m (MRPL23), mL45 (MRPL45) and mL37 (MRPL37), and the 16S RNA, sharing with them a total interface area as large as ≈ 5100 Å^2 (Fig. 4, S3).

Leu91 in MRPL24 is located at the basis of a beta-loop-beta (or beta hairpin) structural motif encompassing residues Thr93-Glu112. This motif provides extensive contacts with the protein mL45 (MRPL45) and the 16S RNA (specifically with its residues 1800–1810) (Fig. S3). The value assumed by the Leu91 ϕ angle in MRPL24 (−147°) is clearly incompatible with the presence of a Pro, which has the ϕ angle restricted around −63° (± 15°) (MacArthur and Thornton, 1991). This implies that the Leu91Pro mutation will cause a conformational change on the protein main chain that will likely affect the orientation of the following beta hairpin motif (Fig. 4) and downstream. The aberrant folding of mutated MRPL24 may lead to reduced steady-state levels, consistent with the above data (Fig. 2a and 3a). < it is expected to result in a less efficient interaction of mutant MRPL24 with other components of the mitoribosome, especially mL45 (MRPL45) and 16S rRNA. A defective interaction between its molecular components can cause, in turn, a disturbance in the 39S mitoribosomal subunit assembly.

3.5. Mitoribosome integrity analysis

Next we set out to analyze the integrity of the mitochondrial ribosomal large subunit in the patient fibroblasts. Upon western blot analysis of whole cell homogenates, we observed decreased levels mitoribosomal proteins MRPL41 and MRPL45 (both of which are positioned adjacent to MRPL24) in patient cells when compared to control cells (Fig. 5a-b). Similarly, upon sucrose density gradient fractionation, we observed decreased levels of MRPL24, MRPL41 and MRPL45 in the fractions corresponding to the large subunit of the mitoribosome (Fig. 5c-e, fractions 6–8). This suggests the large subunit is structurally compromised by the Leu91Pro mutation in *MRPL24*, which may explain the observed phenotype and poor mitochondrial translation activity.

3.6. Functional studies in zebrafish

MRPL24 in human and *Danio rerio* presents about 70% of identity for both protein and mRNA (Fig. 1c) with a high degree of synteny. By qRT-PCR studies, we observed that *mrpl24* had the highest levels of expression at 72 hpf (Fig. 6a) and it was expressed until 120 hpf, albeit to a lesser extent. WISH showed *mrpl24* mRNA signals ubiquitously expressed at 48hpf (Fig. 6b), whereas expression was restricted to somites, brain, heart, and liver at 96 hpf (Fig. 6c-e), suggesting a higher expression in metabolically active tissues.

Using a specific spliceMO, we observed minimal death rate and no morphological changes until 48 hpf when MO-injected embryos showed smaller size, less pigmentation, a slight curvature of the body, and occasionally, heart edema (Fig. 7a) associated with a reduction of

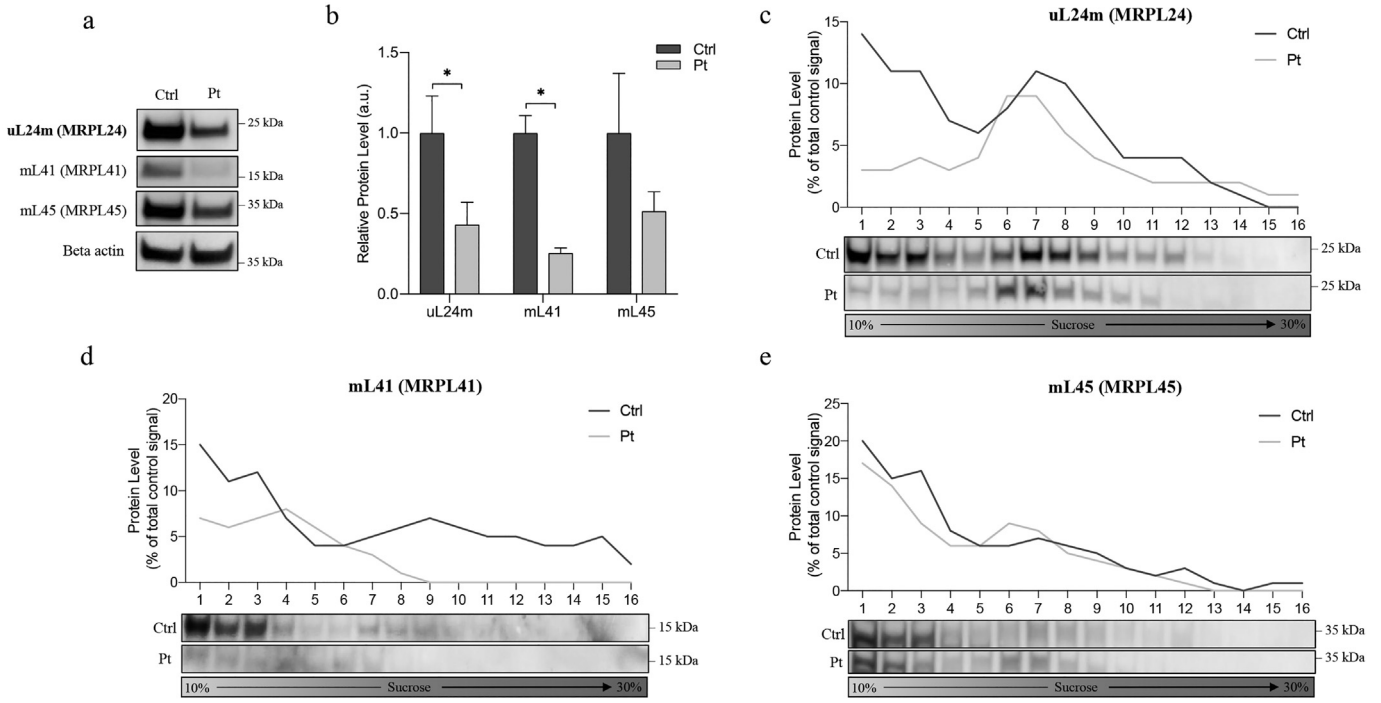

Fig. 5. Effect of MRPL24 mutation on the mitochondrial ribosome. a. Western blot analysis of fibroblast homogenate from control (Ctrl, n = 3) and MRPL24 patient (Pt, n = 3) samples. b. Quantification of band intensities in (a) using ImageJ normalized to Beta actin. Data are presented as mean ± SEM; *$p < .05$. c-e. Sucrose density gradient fractionation and western blot analysis of mitoribosomal large subunit proteins in Ctrl and Pt samples. Quantification of band intensities using ImageJ normalized against the fraction of the total signal relative to control cells.

mRNA expression and protein level (Fig. S4a-b). Over 80% of 48 hpf morphants showed altered touch evoked response test, and unlike the wild-type could not run-off the visual field in a longer registration of their locomotion (Fig. 7b, video S1,2). Contrary to WT larvae, 120 hpf morphants were slowly moving or paralyzed (video S3,4). The alterations of the locomotion at 48hpf were rescued after the co-injection of the WT zebrafish *mrpl24* cRNA (Fig. 7c). A similar effect was obtained by complementing the touch evoked response phenotype of the morphants with WT human but not with the mut^{Leu91Pro} cRNA, suggesting that the Leu91Pro allele is likely deleterious and acts with a loss of function mechanism (Fig. 8).

Like human mutant cells, 48 hpf *mrpl24* morphants showed reduced basal respiration rates and impaired ATP production compared to WT siblings by microscale-oxygraphy (Fig. 9a,b) and had low expression of MRC complexes I and V when tested by Western blotting (Fig. S5). To assess how knocking-down *mrpl24* would impair organ developments, we injected 3 ng spliceMO in a transgenic zebrafish line expressing GFP under the promoter of *myl7,* at the level of cardiomyocytes and performed morphological examination of heart structure and birefringence assay. While we did not observe obvious alterations in birefringence assay (data not shown), 72 hpf morphant embryos presented a slight but significant increase of cardiac edema with an elongated and string-like heart tube, a feature not appearing in WT siblings (Fig. S6). The cardiac phenotype was complemented by co-injection of MO with the mut^{Leu91Pro} cRNA (Fig. 9c). Hepatic size was also increased in 5 dpf morphants with a significant level of lipid storage, a finding suggesting the presence of liver steatosis (Fig. 9d,e).

4. Discussion

Here we report the first case of a patient harboring a mutation in the *MRPL24* gene, which codes for a structural protein of the mitochondrial large ribosomal subunit. Mitoribosomes comprise a 28S small subunit (SSU) made of 12S rRNA and about 30 proteins, and a 39S large subunit (LSU) composed of 16S rRNA and approximately 52 proteins (Greber and Ban, 2016). As a rule, the small subunit is implicated in the decoding of mRNAs, while the large subunit carries out the peptidyltransferase activity for peptide formation (Bieri et al., 2018). In recent years, most of yeast and mammalian mitoribosomal proteins have been identified and further confirmed as components of the mitochondrial ribosome by high-resolution cryo-electron microscopy structures (De Silva et al., 2015; Greber and Ban, 2016). Moreover, it has been reported that these proteins not only have a structural role but also biological functions in translation (Brodersen and Nissen, 2005), even if the exact function of many of them is not yet clear. A hallmark of the mitochondrial ribosome is that, despite the proteobacterial origin, during evolution, certain ribosomal RNA segments have been lost and replaced by mitochondria-specific ribosomal proteins (Smits et al., 2007; Desmond et al., 2011) and this structural change was accompanied by the acquisition of specialized functions for the synthesis of a small set of highly hydrophobic mitochondrial inner membrane proteins (Ott and Herrmann, 2010).

Of the 82 proteins components of the human mitoribosome, up to now only 10 have been linked to mitochondrial diseases: MRPS2 (Gardeitchik et al., 2018), MRPS7 (Menezes et al., 2015), MRPS16 (Miller et al., 2004), MRPS22 (Saada et al., 2007; Smits et al., 2011; Baertling et al., 2015), MRPS23 (Kohda et al., 2016), MRPS25 (Bugiardini et al., 2019), MRPS34 (Lake et al., 2018) of the mt-SSU and MRPL3 (Galmiche et al., 2011), MRPL12 (Serre et al., 2013) and MRPL44 (Carroll et al., 2013; Distelmaier et al., 2015) of the mt-LSU. Defects in these proteins cause heterogeneous and multi-systemic clinical phenotypes, ranging from features common to almost all the described cases, which include severe lactic acidosis, combined OXPHOS deficiency, hypotonia and developmental delay, to specific clinical presentations such as cardiomyopathy (Galmiche et al., 2011; Smits et al., 2011; Carroll et al., 2013; Distelmaier et al., 2015), neurodevelopmental disabilities (Miller et al., 2004; Distelmaier et al., 2015; Lake et al., 2018), corpus callosum agenesis (Saada et al., 2007), Leigh syndrome (Lake et al., 2018), hypoglycemia (Kohda et al., 2016; Gardeitchik et al., 2018), or growth delay and dysmorphic features

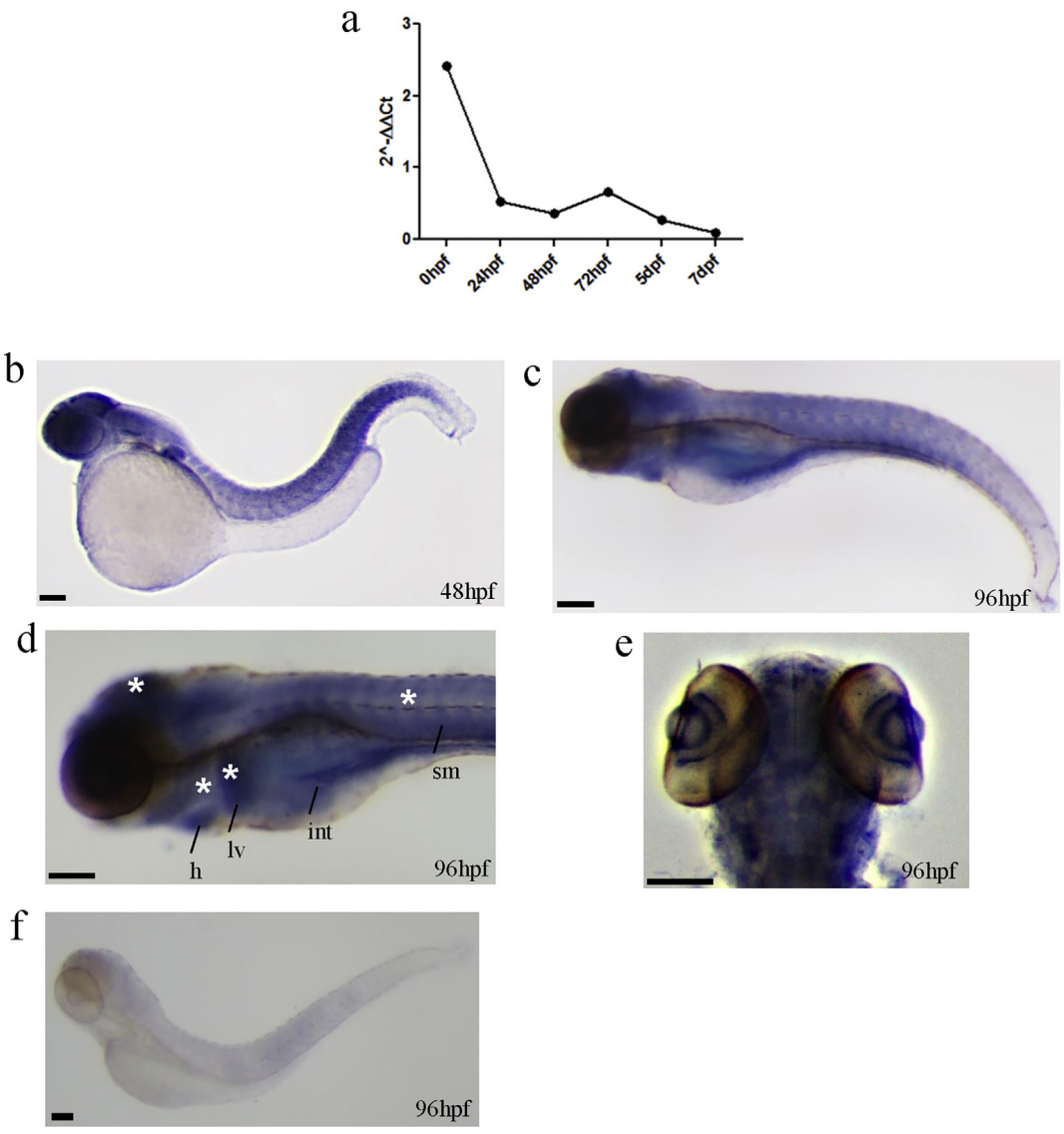

Fig. 6. a. qRT-PCR analysis showing the expression of *mrpl24* until 120 hpf, with highest levels of expression at 72 hpf. b. In situ-hybridization reavealing that *mrpl24* mRNA is ubiquitously expressed at 48hpf, whereas, expression was restricted to somites (*, sm), brain (*), heart (*, h), intestine (int), and liver (*, liv) at 96 hpf (c-e), compared to the sense probe (f).

(Saada et al., 2007; Smits et al., 2011; Lake et al., 2018; Gardeitchik et al., 2018). Here we describe a patient presenting hyperintense bilateral alterations at the level of the putamen, cerebellar atrophy and choreoathetosis of limbs and face with a spastic-dystonic tetraparesis. Moreover, the electrocardiogram disclosed a RS of 91 bpm and ventricular pre-excitation with associated repolarization anomalies. RCC analysis in muscle biopsy revealed a defect of complex IV activity, associated with decreased level of complexes I, IV and V subunits. The amount of MRPL24 protein was reduced both in muscle and fibroblasts, causing markedly reduced levels of the assembled mitochondrial ribosome large subunit and reduced translation of all the mtDNA-encoded subunits. These results provided evidence of the deleterious effect of the p.Leu91Pro *MRPL24* variant in the mitochondrial translation process. To support this, a structural analysis in the context of the human mitoribosome has been performed. MRPL24 is highly interconnected with other proteins and with the 16S RNA within the LSU subunit contributing, together with mL41 (MRPL41), uL23m (MRPL23), uL29m (MRPL47) and bL34m (MRPL34), to the formation of the peptide exit tunnel (Amunts et al., 2015; Bogenhagen et al., 2018). The exit tunnel of the mammalian LSU subunit differs from that of the bacterial 50S subunit due to the loss of two rRNAs and the addition of the mitochondria-specific protein mL45 (MRPL45) and extensions of uL23m (MRPL23), uL24m (MRPL24), and uL29m (MRPL29) (Brown et al., 2014; Greber and Ban, 2016). mL45 (MRPL45) likely anchors the mitoribosome to the inner mitochondrial membrane and exposes the translated nascent polypeptide to solvent (Greber et al., 2014a, 2014b; Brown et al., 2014). The mutation we characterized in MRPL24 is immediately upstream to a conserved beta hairpin structural motif that is in close contact with mL45 (MRPL45) (Brown et al., 2014). A proline in this positionis incompatible with the structure of the wild-type protein, thus necessarily leading to an aberrant folding and, consequently, to an aberrant interaction of MRPL24 with other components of the large mitoribosomal subunit. Overall, our data suggests that the Leu91Pro mutation destabilizes MRPL24, leading to reduced incorporation into the mitoribosome and preventing its efficient interaction with neighbouring proteins. As a consequence, the mitochondrial large subunit is also destabilized. A similar effect was observed for the analogous pathogenic mutation Leu214Pro in MRPS2, hypothesized to cause a conformational change leading to a decrease in the steady-state levels of mutant MRPS2, and preventing the assembly of the small mitoribosomal subunit (Gardeitchik et al., 2018).

In addition, we used an in vivo vertebrate system (zebrafish) to

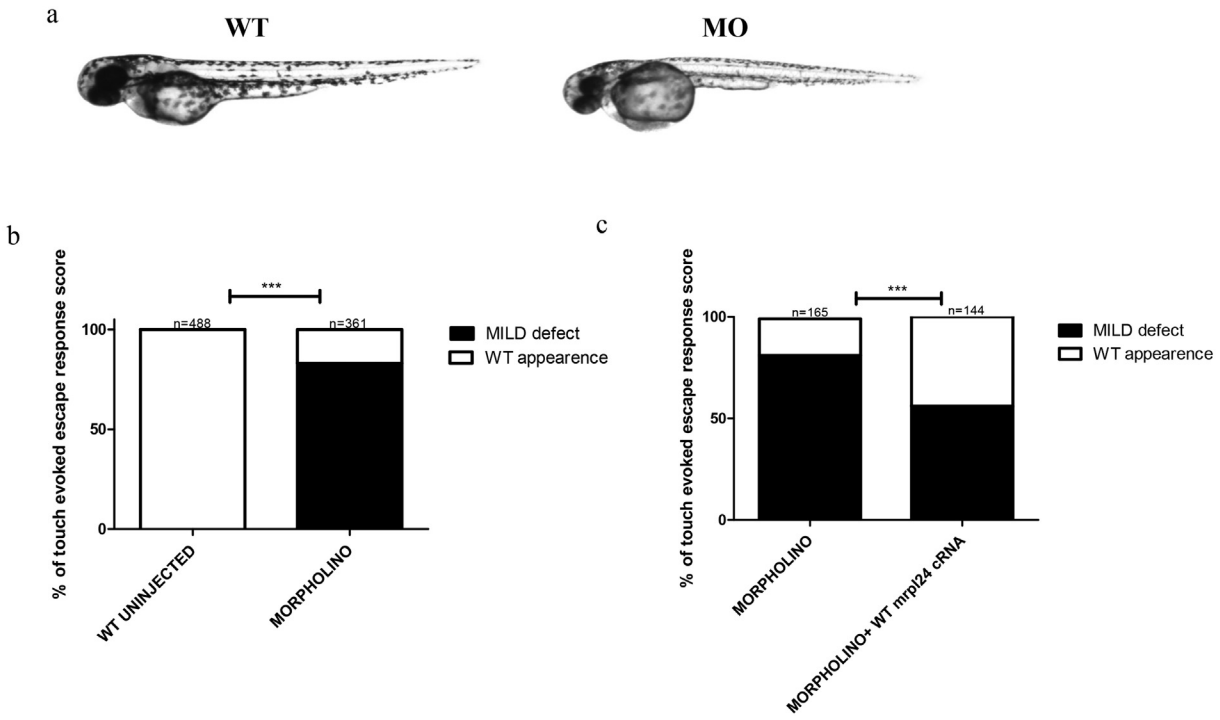

Fig. 7. a. 48 hpf WT and MO-injected embryos, showing the smaller size, decreased pigmentation, slight curvature of the body, and, occasionally, heart edema in the MO. b. Touch evoked response test reveal that over 80% of 48hpf morphants ($n = 361$) showed altered escape response and motility, unlike the wild-type could ($n = 488$). c. Morphant phenotype rescue after the co-injection of the zebrafish *mrpl24* mRNA (MO $n = 165$; MO + WT *mrpl24* cRNA $n = 144$). Each bar represents the mean + s.e.m.; $***p < .0001$; n.s., not significant according to ANOVA with Tukey's Multiple Comparison Test (b) or Unpaired *t*-test (c).

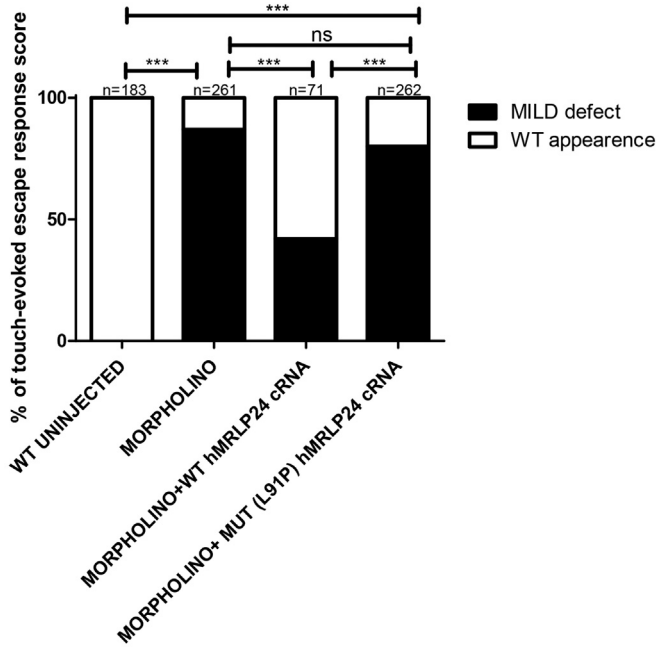

Fig. 8. a. Analysis of the touch evoked response test in uninjected ($n = 183$), morphants ($n = 261$) and MO co-injected with human WT cRNA ($n = 71$), and with human Leu91Pro cRNA ($n = 262$), showing that the mutated mRNA harboring the Leu91Pro mutation did not rescue the phenotype differently than the WT cRNA. $***p < .0001$, n.s., not significant according to Chi-square test.

explore how dysfunctional Mrpl24 interferes with mitochondrial bioenergetics and with organs development, as well as to explore how the identified missense mutation in this gene underlies the pathological effects. In the *mrpl24* knock-down zebrafish embryos, we observed motor impairment and a metabolic damage associated with a considerable reduction of the basal respiration and ATP production, highlighting the presence of mitochondrial dysfunction associated to faulty *mrpl24*. The heterogeneity of MRPs patients is well represented in our model as zebrafish embryos exhibited reduced development, hepatomegaly and lipid accumulation (Howarth et al., 2013; Vacaru et al., 2014). Moreover, we found that MRPL24 has a potential role in cardiac development producing heart impairment. In fact, it has been reported that some MRPs defects gave rise to cardiomyopathy (Galmiche et al., 2011; Smits et al., 2011; Carroll et al., 2013; Distelmaier et al., 2015) or to a large patent ductus arteriosus (Miller et al., 2004). The relatively milder cardiac phenotype observed in our patient could be due to the different mutation (missense in patient, knock-down in zebrafish). However, overexpression of the p.Leu91Pro mutation rescues the heart phenotype of the morphants, but not the locomotion, suggesting that the mutation impacts mainly on motor behavior and less on cardiac function. Conversely, liver involvement, a feature not seen in our proband, could be related to impaired synthesis of ATP in zebrafish directly influencing fatty acid oxidation, steatosis, cell death, and fibrogenesis (Lee and Sokol, 2007). Whilst we cannot speculate on the appearance of liver symptoms in our patient with disease progression, other mutations affecting MRPs have been associated with liver dysfunction (Menezes et al., 2015; Kohda et al., 2016; Lake et al., 2018).

In conclusion, our study demonstrates for the first time that MRPL24 is required for normal mitochondrial function in zebrafish and humans, and that mutations destabilizing this protein underlie the clinical manifestations of mitochondrial dysfunction.

Role of authors

M. Di N., C. D. M., G. T., T. R., E. F-V., C. N.: performed functional analysis on muscle and fibroblasts.

M. M., F. M.: created the morphant zebrafish and performed related functional analysis.

D. V., A. T.: performed NGS, Sanger experiments and the related bioinformatics analyses.

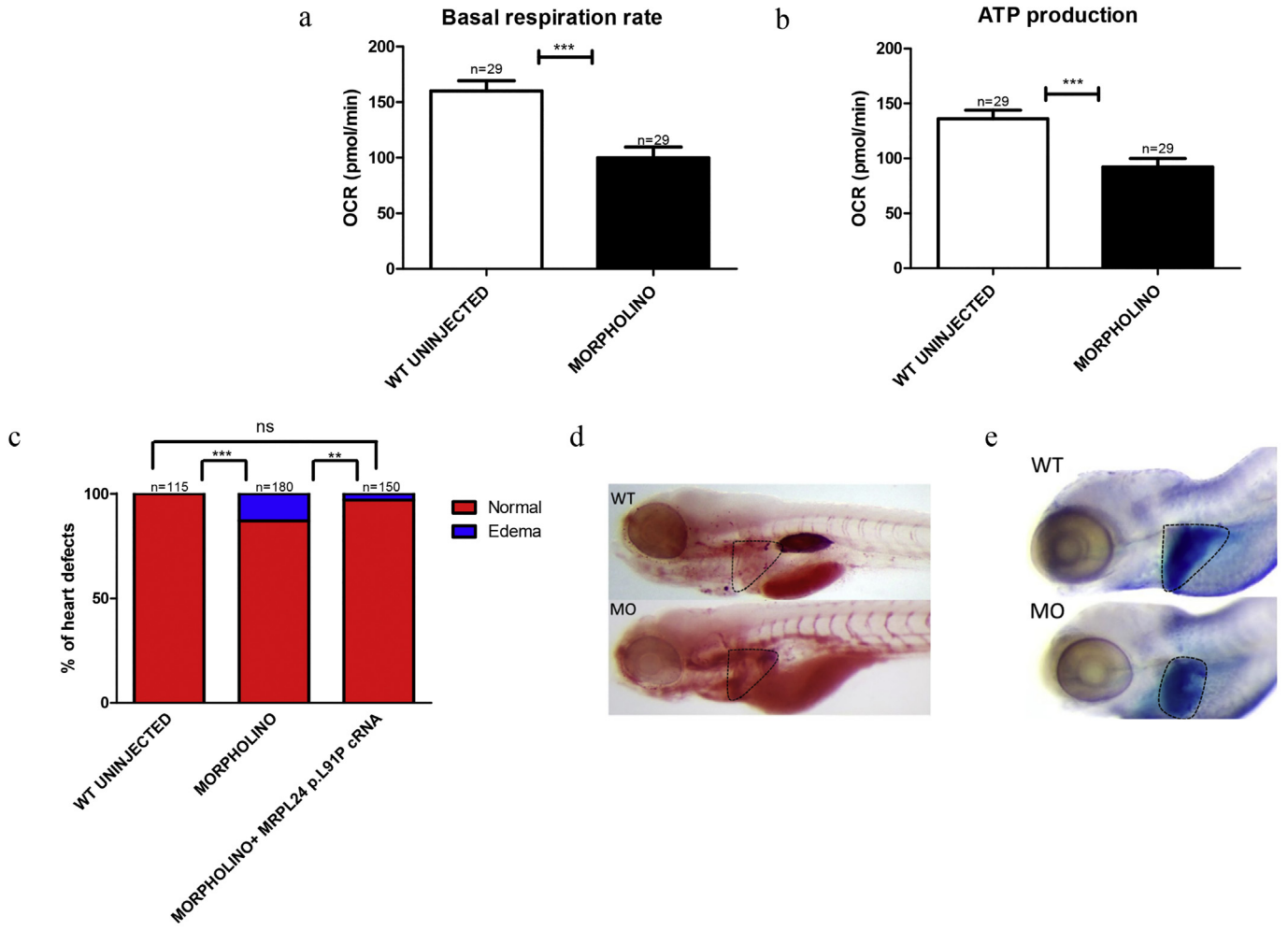

Fig. 9. a-b. Micro-oxygraphy analysis of 48 hpf *mrpl24* morphants ($n = 29$) and control uninjected (n = 29) embryos, showing the reduction of the basal respiration rates and impaired ATP production in morphants. c. The cardiac phenotype was complemented by co-injection of the human mutant Leu91Pro cRNA ($n = 150$). d-e. Morphological examination of heart 72hpf morphants ($n = 180$) presented a slight but significant increase of cardiac edema with an elongated and string-like straight heart tube not appearing in WT siblings ($n = 115$). Moreover, Oil-Red-O staining and in situ hybridization with *fabp10a*, showed significant level of lipid accumulation indicative of steatosis and increased liver size, respectively in morphants. ***$p \leq .0001$, **$p < .001$, n.s., not significant according to Mann–Whitney test (a-b) and to Fisher exact Contingency test (c). (For interpretation of the references to colour in this figure legend, the reader is referred to the web version of this article.)

R. O.: provided model building and analysis on the structure of the mutated protein.

D. G.: performed biochemical study on muscle samples and revised the manuscript.

A. A., G. V., E. B.: Acquisition and analysis of clinical data.

M. Di N., M.M., R. O., R.C.: write the original draft.

M. Z., Mi. M, E. B., F.M. S., R. C.: conceptualization of this study, drafting and editing of the manuscript, analysis and interpretation of data.

All authors: reviewed and edited the final version of the manuscript.

CRediT author statement

The corresponding author ensures that the descriptions of the authors' role is accurate and have been shared with all authors.

M. Di N., M. M., D. V., C. D. M., A. T., R. O., E. F-V., F. M., G. T., T. R., C. N.,: Methodology; Formal analysis.

M. Di N., M. M., D. V., C. M., A. T., R. O., E. F-V., F. M., G. T., T. R., A. A., C. N., G. V.: Investigation.

M. Di N., M.M., R. O., R.C.: writing the original draft.

D. G., M. Z., Mi. M, E. B., F. M. S., R. C.: Writing - Review & Editing.

R. C.: Supervision.

M. M., R. O., D. G. M. Z., Mi. M, E. B., F. M. S., R. C.: Funding acquisition.

Declaration of Competing Interest

None of the authors has any conflicts to disclose.

Acknowledgements

EB and RC are supported by the Italian Ministry of Health Ricerca Corrente; EB is supported also by the Italian Ministry of Health Ricerca Finalizzata (RF-2016-02361241). FMS was partially supported by a grant from Regione Toscana (RR/NUTRA-FISH). DG is supported by the Telethon Foundation (GGP15041). RO thanks MIUR-FFABR (Fondo per il Finanziamento Attività Base di Ricerca) for funding. M.M. was partially supported by the Starting Grant from Italian Minister of Health Ricerca Finalizzata. M.Z. was supported by the Core Grant from the MRC (Grant MC_UU_00015/5); ERC Advanced GrantFP7-322424 and NRJ-Institut de France Grant. Mi.M. and C.D.M. were supported by the Core Grant from the MRC (Grant MC_UU_00015/4). We also thank Dr. Letizia Pitto for technical and scientific assistance at the Italian National Research Council (NRC)-zebrafish core facility.

Appendix A. Supplementary data

Supplementary data to this article can be found online at https://doi.org/10.1016/j.nbd.2020.104880.

References

Amunts, A., et al., 2015. Ribosome. The structure of the human mitochondrial ribosome. Science 348, 95–98.

Baertling, F., et al., 2015. MRPS22 mutation causes fatal neonatal lactic acidosis with brain and heart abnormalities. Neurogenetics 16, 237–240.

Bieri, P., et al., 2018. High-resolution structures of mitochondrial ribosomes and their functional implications. Curr. Opin. Struct. Biol. 49, 44–53.

Bogenhagen, D.F., et al., 2018. Kinetics and mechanism of mammalian mitochondrial ribosome assembly. Cell Rep. 22, 1935–1944.

Brodersen, D.E., Nissen, P., 2005. The social life of ribosomal proteins. FEBS J. 272, 2098–2108.

Brown, A., et al., 2014. Structure of the large ribosomal subunit from human mitochondria. Science 346, 718–722.

Bugiani, M., et al., 2004. Clinical and molecular findings in children with complex I deficiency. Biochim. Biophys. Acta 1659, 136–147.

Bugiardini, E., et al., 2019. MRPS25 mutations impair mitochondrial translation and cause encephalomyopathy. Hum. Mol. Genet. https://doi.org/10.1093/hmg/ddz093.

Calvo, S.E., et al., 2012. Molecular diagnosis of infantile mitochondrial disease with targeted next-generation sequencing. Sci. Transl. Med. 4, 118ra10.

Carroll, C.J., et al., 2013. Whole-exome sequencing identifies a mutation in the mitochondrial ribosome protein MRPL44 to underlie mitochondrial infantile cardiomyopathy. J. Med. Genet. 50, 151–159.

Chomyn, A., 1996. In vivo labeling and analysis of human mitochondrial translation product. Methods Enzymol. 264, 197–211.

De Silva, D., et al., 2015. Mitochondrial ribosome assembly in health and disease. Cell Cycle 14, 2226–2250.

DeLano, W.L., 2002. The PyMOL Molecular Graphics System. Available. http://www.pymol.org (Accessed on 2018 December 3).

Desmond, E., et al., 2011. On the last common ancestor and early evolution of eukaryotes: reconstructing the history of mitochondrial ribosomes. Res. Microbiol. 162, 53–70.

Distelmaier, F., et al., 2015. MRPL44 mutations cause a slowly progressive multisystem disease with childhood-onset hypertrophic cardiomyopathy. Neurogenetics 16, 319–323.

Fernández-Silva, P., et al., 2007. In vivo and in organello analyses of mitochondrial translation. Methods Cell Biol. 80, 571–588.

Fraher, D., et al., 2016. Zebrafish embryonic lipidomic analysis reveals that the yolk cell is metabolically active in processing lipid. Cell Rep. 14, 1317–1329.

Galmiche, L., et al., 2011. Exome sequencing identifies MRPL3 mutation in mitochondrial cardiomyopathy. Hum. Mutat. 32, 1225–1231.

Gardeitchik, T., et al., 2018. Bi-allelic mutations in the mitochondrial ribosomal protein MRPS2 cause sensorineural hearing loss, hypoglycemia, and multiple OXPHOS complex deficiencies. Am. J. Hum. Genet. 102, 685–695.

Gibert, Y., et al., 2013. Metabolic profile analysis of zebrafish embryos. J. Vis. Exp. 14, e4300.

Gopisetty, G., Thangarajan, R., 2016. Mammalian mitochondrial ribosomal small subunit (MRPS) genes: a putative role in human disease. Gene 589, 27–35.

Greber, B.J., Ban, N., 2016. Structure and function of the mitochondrial ribosome. Annu. Rev. Biochem. 85, 103–132.

Greber, B.J., et al., 2014a. Architecture of the large subunit of the mammalian mitochondrial ribosome. Nature 505, 515–519.

Greber, B.J., et al., 2014b. The complete structure of the large subunit of the mammalian mitochondrial ribosome. Nature 515, 283–286.

Greber, B.J., et al., 2015. Ribosome. The complete structure of the 55S mammalian mitochondrial ribosome. Science 348, 303–308.

Howarth, D.L., et al., 2013. Defining hepatic dysfunction parameters in two models of fatty liver disease in zebrafish larvae. Zebrafish 10, 199–210.

Huang, C., et al., 2003. Germ-line transmission of a myocardium-specific GFP transgene reveals critical regulatory elements in the cardiac myosin light chain 2 promoter of zebrafish. Dev. Dyn. 228, 30–40.

Kenmochi, N., et al., 2001. The human mitochondrial ribosomal protein genes: mapping of 54 genes to the chromosomes and implications for human disorders. Genomics 77, 65–70.

Kohda, M., et al., 2016. A comprehensive genomic analysis reveals the genetic landscape of mitochondrial respiratory chain complex deficiencies. PLoS Genet. 12, e1005679.

Lake, N.J., et al., 2018. Biallelic mutations in MRPS34 lead to instability of the small mitoribosomal subunit and Leigh Syndrome. Am. J. Hum. Genet. 102, 713.

Lee, W.S., Sokol, R.J., 2007. Liver disease in mitochondrial disorders. Semin. Liver Dis. 27, 259–273.

MacArthur, M.W., Thornton, J.M., 1991. Influence of proline residues on protein conformation. J. Mol. Biol. 218, 397–412.

Marchese, M., et al., 2016. Dolichol-phosphate mannose synthase depletion in zebrafish leads to dystrophicmuscle with hypoglycosylated α-dystroglycan. Biochem. Biophys. Res. Commun. 477, 137–143.

Menezes, M.J., et al., 2015. Mutation in mitochondrial ribosomal protein S7 (MRPS7) causes congenital sensorineural deafness, progressive hepatic and renal failure and lactic acidemia. Hum. Mol. Genet. 24, 2297–2307.

Miller, C., et al., 2004. Defective mitochondrial translation caused by a ribosomal protein (MRPS16) mutation. Ann. Neurol. 56, 734–738.

O'Brien, T.W., et al., 2000. Mammalian mitochondrial ribosomal proteins (4). Amino acid sequencing, characterization, and identification of corresponding gene sequences. J. Biol. Chem. 275, 18153–18159.

O'Brien, T.W., et al., 2005. Nuclear MRP genes and mitochondrial disease. Gene 354, 147–151.

Ott, M., Herrmann, J.M., 2010. Co-translational membrane insertion of mitochondrially encoded proteins. Biochim. Biophys. Acta 1803, 767–775.

Rizza, T., et al., 2009. Assaying ATP synthesis in cultured cells: a valuable tool for the diagnosis of patients with mitochondrial disorders. Biochem. Biophys. Res. Commun. 383, 58–62.

Rorbach, J., et al., 2016. Human mitochondrial ribosomes can switch their structural RNA composition. Proc. Natl. Acad. Sci. U. S. A. 113, 12198–12201.

Saada, A., et al., 2007. Antenatal mitochondrial disease caused by mitochondrial ribosomal protein (MRPS22) mutation. J. Med. Genet. 44, 784–786.

Sali, A., Blundell, T.L., 1993. Comparative protein modelling by satisfaction of spatial restraints. J. Mol. Biol. 234, 779–815.

Serre, V., et al., 2013. Mutations in mitochondrial ribosomal protein MRPL12 leads to growth retardation, neurological deterioration and mitochondrial translation deficiency. Biochim. Biophys. Acta 1832, 1304–1312.

Smith, L.L., et al., 2013. Analysis of skeletal muscle defects in larval zebrafish by birefringence and touch-evoke escape response assays. J. Vis. Exp. 82, e50925.

Smits, P., et al., 2007. Reconstructing the evolution of the mitochondrial ribosomal proteome. Nucleic Acids Res. 35, 4686–4703.

Smits, P., et al., 2011. Mutation in mitochondrial ribosomal protein MRPS22 leads to Cornelia de Lange-like phenotype, brain abnormalities and hypertrophic cardiomyopathy. Eur. J. Hum. Genet. 19, 394–399.

Spirina, O., et al., 2000. Heart-specific splice-variant of a human mitochondrial ribosomal protein (mRNA processing; tissue specific splicing). Gene 261, 229–234.

Thisse, C., Thisse, B., 2008. High-resolution in situ hybridization to whole-mount zebrafish embryos. Nat. Protoc. 3, 59–69.

Tolomeo, D., et al., 2019. Clinical and neuroimaging features of the m.10197G > A mtDNA mutation: new case reports and expansion of the phenotype variability. J. Neurol. Sci. 399, 69–75.

Torraco, A., et al., 2018. ISCA1 mutation in a patient with infantile-onset leukodystrophy causes defects in mitochondrial [4Fe-4S] proteins. Hum. Mol. Genet. 27, 3650.

Vacaru, A.M., et al., 2014. Molecularly defined unfolded protein response subclasses have distinct correlations with fatty liver disease in zebrafish. Dis. Model. Mech. 7, 823–835.

Vangone, A., et al., 2011. COCOMAPS: a web application to analyze and visualize contacts at the interface of biomolecular complexes. Bioinformatics 27, 2915–2916.

Westerfield, M., 2000. The Zebrafish Book. A Guide for the Laboratory Use of Zebrafish (*Danio rerio*), 4th edition. University of Oregon Press, Eugene.